Promoting Strong Metal Support Interaction: Doping ZnO for Enhanced Activity of Cu/ZnO:M (M = Al, Ga, Mg) Catalysts

Julia Schumann, Maik Eichelbaum,* Thomas Lunkenbein, Nygil Thomas,[†] Maria Consuelo Álvarez Galván,[‡] Robert Schlögl,[§] and Malte Behrens*[,||]

Department of Inorganic Chemistry, Fritz-Haber-Institut der Max-Planck-Gesellschaft, Faradayweg 4-6, 14195 Berlin, Germany

Ⓢ Supporting Information

ABSTRACT: The promoting effect of Al, Ga, and Mg on the support in Cu/ZnO catalysts for methanol synthesis has been investigated. Different unpromoted and promoted ZnO supports were synthesized and impregnated with Cu metal in a subsequent step. All materials, supports, and calcined and activated catalysts were characterized by various methods, including contactless (microwave) conductivity measurements under different gas atmospheres. Small amounts of promoters were found to exhibit a significant influence on the properties of the oxide support, concerning textural as well as electronic properties. We found correlations between the conductivity of the ZnO support and the activity of the catalyst in the reverse water-gas shift reaction (rWGS) as well as in methanol synthesis. In rWGS the activation energy and reaction order in H_2 are decreased upon promotion of the ZnO support with the trivalent promoters Al^{3+} and Ga^{3+}, indicating an electronic promotion. In methanol synthesis, results point to a structural promotion by Al^{3+} and Ga^{3+}. A detrimental effect of Mg^{2+} doping was observed in both reactions. This effect is discussed in the context of the reducibility of ZnO under reaction conditions, which can be tuned by the promoter in different ways. The reducibility is seen as a critical property for the dynamic metal support interaction of the Cu/ZnO system.

KEYWORDS: ZnO, Cu, methanol synthesis, rWGS, promotion, conductivity
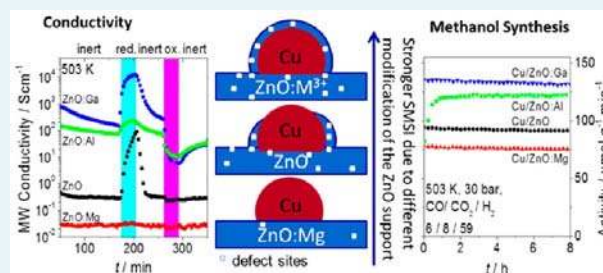
■ INTRODUCTION

Cu/ZnO/Al$_2$O$_3$ catalysts are used industrially for methanol synthesis, one of the most important industrial processes in syngas chemistry. Cu is commonly regarded as the active phase, but the role of ZnO and Al$_2$O$_3$ is more than that of an inert support.[1] For a long time a synergistic effect of Cu and ZnO has been debated and different origins of the synergy have been discussed.[2] A hydrogen spillover mechanism, where ZnO acts as a reservoir for hydrogen facilitating the hydrogenation over adjacent Cu surfaces,[3] or the so-called strong metal support interaction (SMSI), which leads to a wetting of the ZnO under reducing atmosphere, covering the Cu particles and leading either to morphology changes[1c,4] or supply of Zn atoms to the copper surface,[5] were considered. Recently the Cu/ZnO synergy was confirmed by a combined microscopic and theoretical study to result from a Zn species being an integral part of the active site in methanol synthesis, sitting on highly active Cu steps.[1a]

Less has been reported about the promotional effect of Al, which is still not very well understood. In general, small amounts of substances added to a catalyst are called promoters if they beneficially affect the activity by modifying the physical structure, such as crystallinity, surface or pore size, or the electronic structure of the catalyst.[6] We assume that structural promoters increase the number of active sites but only electronic promoters would have, through modification of the active site, an influence on the activation energy and reaction order of a catalytic reaction.

In Cu/ZnO catalyst preparations alumina was found to be a component that improves the morphology and stability of the catalysts as a structural promoter.[7] On the other hand, small amounts of Al^{3+} also change the metal surface area normalized activity of Cu/ZnO catalysts in methanol synthesis.[8] NMR spectroscopy revealed that small amounts of Al^{3+} are actually incorporated into the ZnO lattice, occupying tetrahedrally coordinated sites,[9] similar to the case in doped semiconductors for optical applications and are thus not assumed to modify the active copper part of the catalyst.

The popularity of ZnO in semiconductor applications derives from its convenient properties such as the direct wide band gap (3.3 eV) and the large exciton energy (60 meV), which render ZnO especially promising for optoelectronic applications.[10] For the preparation of n-type ZnO, doping with group XIII elements such as Al^{3+} and Ga^{3+} is commonly applied in order to increase conductivity and alter the electronic structure.[10] The effect of these doped ZnO species on the aforementioned SMSI effect in Cu/ZnO has not yet been resolved.

Herein, we report a model study to better understand whether the electronic structure of ZnO altered by promoters such as Al^{3+} or Ga^{3+} influences the extent of the SMSI with Cu for the reverse

water-gas shift (rWGS) or the methanol synthesis. Therefore, we decouple the promotion from the typical hydroxy-carbonate precursor chemistry commonly applied to the preparation of industrial Cu/ZnO:Al catalysts and synthesized doped model supports ZnO:M (M = Al, Ga, Mg) without Cu. These supports were thoroughly characterized before and after loading with the copper phase in a subsequent step by impregnation. By contactless conductivity measurements and UV–visible spectroscopy, among other characterization techniques, insights were gained into the electronic structure of the support and the role of different promoters. The impregnated support was tested in the rWGS reaction and methanol synthesis, and the catalytic data were correlated with the electronic properties.

■ EXPERIMENTAL SECTION

Sample Preparation. Differently promoted ZnO supports (3 mol % M: Al, Ga, Mg) were prepared by (co-) precipitation of the appropriate amount of metal nitrates (1 M) and Na_2CO_3 solution (1.6 M) at 338 K and pH 6.5 in an automated reactor (Labmax; see Figure S1 in the Supporting Information for the recorded preparation protocol of the precursor phase). The precipitate was aged, washed, spray-dried, and calcined at 603 K (2 K min^{-1}, dwell time 180 min). The promoter amount of 3% based on $[M^{2/3+}]/([M^{2/3+}]+[Zn])$ was shown previously to lead to a significant change in structural and catalytic properties.[8,9] Copper was impregnated on the ZnO samples using the copper citrate route: Cu citrate ($Cu_2C_6H_4O_7 \cdot 2.5H_2O$) was dissolved in a 12.5 vol % aqueous ammonia solution, 2 mL of copper-containing solution was added to 1 g of support, and the slurry was stirred and dried overnight and calcined at 603 K under a static environment (2 K min^{-1} heating ramp, 180 min), resulting in a Cu loading of approximately 10%. In case of unpromoted ZnO also 5 and 15% Cu loadings were prepared.

Characterization Methods. Powder X-ray diffraction (XRD) patterns of the calcined samples were recorded on a STOE Stadi-P diffractometer equipped with a primary focusing Ge monochromator (Cu $K\alpha_1$ radiation) and a linear-position-sensitive detector. The sample was mounted in the form of a clamped sandwich of small amounts of powder fixed with a small amount of grease between two layers of thin polyacetate film. Pattern fitting and phase analysis were carried out using the Rietveld method as implemented in the TOPAS software package.[11] X-ray fluorescence spectroscopy (XRF) was performed in a Bruker S4 Pioneer X-ray spectrometer.

Temperature-programmed reduction (TPR) of the calcined sample was performed in a fixed bed reactor (TPDRO-1100, CE instruments), in 5 vol % H_2 in argon at a heating rate of 6 K min^{-1} (40 mL min^{-1}, end temperature 623 K, holding time 30 min). The H_2 consumption was monitored with a thermal conductivity detector.

Specific surface areas were determined by N_2 physisorption in a Quantachrome Autosorb-1 machine. Prior to analysis, the samples were degassed for 2 h at 353 K. N_2O chemisorption capacities were determined using the N_2O-reactive frontal chromatography (RFC) method.[12] Approximately 100 mg of calcined sample (sieve fraction) was placed in a fixed bed reactor; after in situ reduction, 10 mL/min of a 1% N_2O in He mixture was used at room temperature. The N_2O capacity and the apparent Cu-SA_{N_2O} were calculated from the MS signal of the N_2 trace (m/z 28). H_2-transient adsorption (TA) was performed in the same setup that was used for N_2O-RFC and performed similarly as described in ref 13. For approximately 100 mg of the sample, H_2-TA was recorded at room temperature under 20 mL/min 5% H_2 in Ar for 1 h for the calcined sample (CuO), the reduced sample (Cu), and the sample after N_2O-RFC (Cu_2O) after thorough purging in argon. Under the assumption that H_2 reacts only with surface Cu_2O, the area between the Cu and Cu_2O transient adsorption branch was integrated and the amount of consumed H_2 was quantified to deduce the Cu-$SA_{H_2,TA}$ value.

Scanning electron microscopy (SEM) images were taken on a Hitachi S-4800 field emission gun (FEG) system. High angle annular dark field scanning transmission electron microscopy (HAADF-STEM) images were taken on a FEI Titan 80-300 instrument equipped with a Cs

corrector at 300 kV. Prior to TEM investigation, the sample was reduced up to 523 K and transferred with a vacuum transfer holder (GATAN) under inert conditions to the microscope.

UV–vis–NIR spectroscopy was performed under in situ conditions. UV–vis spectroscopy was recorded on a PerkinElmer Lambda 650 high performance spectrometer equipped with a Harrick Praying Mantis diffuse reflectance attachment and a high-temperature (up to 923 K) in situ cell, which was connected to a gas delivery system. The band gap energy was calculated by linear extrapolation of the function $[[F(R)] h\nu]^{1/2}$ versus $h\nu$ to 0, as suggested by Weber[14] and Iglesia and co-workers.[15] This procedure results from a linearization of the theory of direct and indirect band gap transitions in semiconductors[16] and has been explained in detail by Barton et al.[15c]

The reduced catalyst was characterized by X-ray photoelectron spectroscopy (XPS) at the ISISS beamline of the synchrotron facility BESSY-II of the Helmholtz-Zentrum Berlin (HZB). The samples were mounted in the glovebox and transferred under inert conditions. A depth profiling experiment was performed to estimate the distribution of the metals as a function of information depth. To do so, Cu 3p, Zn 3p and Al 2p, Mg 2p, Ga 3d core levels were recorded at various photon energies, yielding electron kinetic energies of 180, 400, 800, and 1100 eV.

Methanol synthesis from syngas and CO_2/H_2 feeds was tested in a fixed bed flow reactor. A 50 mg portion of the sample (100−200 μm, diluted with 0.7 g of SiO_2) was loaded into a 6 mm inner diameter stainless steel reactor tube. The catalysts were reduced at 523 K (1 K min^{-1}) for 1.5 h in 20% H_2 in Ar. Upon completion of the reduction, the reactor was cooled to 503 K, and a 3/1 H_2/CO_2 mixture (100 mL min^{-1}) containing 4% Ar (as internal standard) was introduced into the reactor. Online analysis of products was performed with a gas chromatograph (Agilent 7890A). Performance under syngas conditions was tested in the same setup after increasing the pressure to 30 bar. The feed gas contained 6% CO, 8% CO_2, 59% H_2, and balance of inert gas.

RWGS was carried out also under a H_2/CO_2 1/1 gas mixture in an 8-fold parallel reactor setup. Tubular quartz glass reactors with an inner diameter of 6 mm were used. Each reactor was placed inside a programmable furnace, and the temperatures were measured using type K thermocouples placed in the catalyst beds. A 50 mg portion of the catalyst was diluted with SiC, to improve heat transport and prevent hot-spot formation. Prior to the activity tests, the samples were reduced in situ under a 5% H_2 in N_2 flow (30 mL/min) with a heating ramp of 1 K min^{-1} to 523 K and a holding time of 30 min.

Conductivity measurements were performed by applying the contact-free and noninvasive microwave cavity perturbation technique. The newly developed conductivity setup and the measurement principle have been described in detail recently[17] and allow the investigation of the charge transport at microwave frequencies in catalysts in a fixed bed reactor at elevated temperatures. As resonator a cylindrical X-band TM_{110} silver-plated brass cavity (ZWG Berlin-Adlershof; resonance frequency 9.2 GHz) with a height of 19.5 mm and a diameter of 38.5 mm was used. A quartz tube reactor with 4 mm outer and 3 mm inner diameter containing the sample under investigation (100−200 μm sieve fraction of pressed and sieved ZnO powder samples, catalyst bed length 10 mm, fixed with quartz wool plugs), surrounded by a 10 mm outer diameter double-walled evacuated quartz Dewar mantle to protect the resonator from convection heat, was directly placed in the center of the cavity. This quartz tube flow-through reactor was connected upstream to a gas delivery manifold equipped with mass flow controllers (Bronkhorst El-Flow) to supply the different gas mixtures with a total flow of 20 mL/ min. Heating of the reactor was performed by preheating a stream of 8 L/min N_2 gas in a resistive furnace consisting of a Sylvania tungsten Series I heater. Downstream of the heater, the N_2 stream was flowing between the quartz Dewar mantle and the outer wall of the reactor tube. The temperature at the catalyst was controlled by a type K thermocouple inside the reactor and a PID controller (Eurotherm 3216) regulating the furnace. The cavity was connected via a W90 wave guide and a flexible SMA coaxial cable with a vector network analyzer (Agilent PNA-L N5230C-225) in order to record resonance spectra of S11 parameters in reflection mode (microwave power attenuation 11 dBm). With a Smith chart analysis of the complex reflection factor and
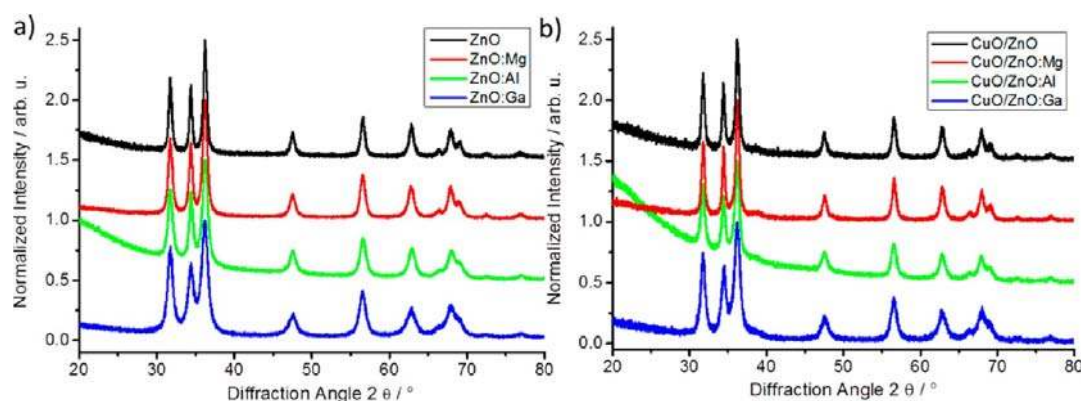
Figure 1. XRD patterns of (a) ZnO:M and (b) CuO/ZnO:M (M = Mg, Al, Ga).

by application of transmission line theory the unloaded quality factor and resonance frequency were deduced for every measurement point. From the change of the quality factor with and without sample the imaginary part of the effective permittivity was calculated. After the Landau−Lifshitz−Looyenga effective medium theory was applied, the permittivity of the solid and finally the conductivity were calculated.[17b]

Continuous-wave EPR spectra were recorded on a Bruker ESP 300 E spectrometer operating in the X-band frequency range and equipped with a Bruker ER 4116 DM (TE102 mode) resonator and a Bruker ER 042 MRH E microwave bridge. Samples were measured in Wilmad quartz (CFQ) EPR tubes (4 mm o.d.) at 293 K using a microwave frequency of ca. 9.64 GHz, a microwave power of 20 mW, a modulation frequency of 100 kHz, and a modulation amplitude of 0.95 G. The microwave frequency was measured with an Agilent 53150A 20 GHz Microwave Frequency Counter. For a quantitative comparison of the signal intensities of the different samples, an external Cr^{3+}/MgO standard (in a thin capillary) was introduced into the resonator in addition to the sample tube. The shown and evaluated EPR spectra were normalized to the maximum of the Cr^{3+} signal (at a g factor of 1.9796) of this standard.

RESULTS AND DISCUSSION

Zinc-hydroxy carbonate precursor phases with and without 3 mol % (based on $[M^{3+/2+}]+[Zn^{2+}]$) of Al^{3+}, Ga^{3+}, or Mg^{2+} promoters were synthesized by coprecipitation. Calcination at 603 K yielded nanocrystalline ZnO (see Figure 1a). In XRD no crystalline minor phases were observed, which indicates that the added promoters do not form crystalline segregated biphases, and should be incorporated into the ZnO crystal lattice. The calculated lattice parameters from Rietveld refinement are given in the Supporting Information (see Table S1). Several effects of promoter incorporation were observed for different promoting ions. Incorporation of Al^{3+} led to a slight contraction of the unit cell, which agrees with the assumption that Al^{3+}, with a smaller effective ionic radius (IR = 0.39 Å[18]), replaces Zn^{2+} (IR = 0.60 Å[18]) on tetrahedral sites. It was also shown before by solid state NMR that at an Al content of 3% a substantial fraction of Al^{3+} ions occupy tetrahedrally coordinated sites in the ZnO structure.[9] Similar solubility limits of Al^{3+} in ZnO were reported by other groups,[19] although much lower limits have been also reported using different preparation routes.[20] In contrast, for Ga incorporation into ZnO an expansion of the lattice parameter a and the cell volume was observed. Ga^{3+} (IR = 0.47 Å[18]) has a larger ionic radius than Al^{3+} (0.39 Å) and thus might occupy the larger octahedral sites.[21] In literature values as high as 20% Ga incorporation into ZnO without biphase formation have been reported.[22] ZnO:Mg displayed lattice constants closest to those of the unpromoted sample, as Mg^{2+} also is the most similar with

respect to size (IR = 0.57 Å[18]) and valency to Zn^{2+}. It was reported that MgO forms a separate phase at 10%, but for 5% Mg, single-phase ZnO was reported.[23]

A significant influence of the promoter on the ZnO morphology was observed. Calculated ZnO domain sizes were between 7 and 13 nm, with the unpromoted ZnO having the largest domain size, Mg- and Al-promoted ZnO having slightly decreased domain sizes, and Ga-promoted ZnO having the smallest domain size, decreased by 50% in comparison to the unpromoted sample (see Figure 1 and Table 1). The promoter-induced defects seem to hinder large particle growth or destroy the long-range crystallographic order.

Table 1. Sample Characterization of Bare Supports and Impregnated Catalysts

	domain size ZnO[a] (pure support) (nm)	BET of support $(m^2 g^{-1})$	domain size ZnO[a] after impreg (nm)	BET after impreg $(m^2 g^{-1})$
ZnO	12.9	41	13.0	34 ± 2
ZnO:Mg	9.9	60	12.7	47 ± 5
ZnO:Ga	6.7	95	7.9	52 ± 4
ZnO:Al	9.5	89	10.5	45 ± 2

[a]Lvol-IB value as determined from Rietveld fit.

After the impregnation with 10% of Cu and a further calcination step, the samples showed only small differences in the XRD pattern, in comparison to the state before the impregnation with CuO (see Figure 1). Only very weak broad signals can be seen, where the CuO (111) reflection is expected at around 38.6° 2θ, which indicated that the copper oxide is finely dispersed. Rietveld fitting resulted in small CuO domain sizes of 2−5 nm. ZnO domain sizes were slightly increased with values between 8 and 13 nm (see Figure 1b and Table 1). After reduction the lattice parameters and domain size of ZnO and Cu/ZnO do not change significantly (see Table S1 in the Supporting Information). The metallic Cu particles of Cu/ZnO have a domain size of around 4 nm. The respective diffractograms are shown in Figure S2 in the Supporting Information.

The accessible surface area (SA), measured by N_2 physisorption (BET), reflects well the trend already observed for the ZnO domain sizes. The unpromoted sample with the largest domain sizes exhibited the smallest surface area, whereas ZnO:Ga had the largest surface area (see Table 1). Doping with Mg^{2+} increased the SA slightly in comparison to the unpromoted sample, and promotion with Ga^{3+} and Al^{3+} more than doubled

the SA. After impregnation with Cu the BET surface area was reduced for all samples and the differences between the differently promoted samples were no longer that great. The amount of Cu loaded onto the support was checked with XRF measurements and found to be close to the nominal value (Table 2). The small deviations in Cu loading probably originate from

Table 2. Cu Content, Surface Capacities, and Cu-SA Determined by N_2O-RFC and H_2-TA and ZnO Defects after Reduction to 523 K

	Cu added by impreg[a] (wt %) (nominal value 10%)	N_2O capacity ($\mu mol\,g^{-1}$) (($m^2\,g^{-1}$)[b])	H_2-TA[c] ($\mu mol\,g^{-1}$) (($m^2\,g^{-1}$))	ZnO defects ($\mu mol\,g^{-1}$)
Cu/ZnO	9.4	67 (5.7 ± 0.2)	50 (4.1)	17
Cu/ZnO:Mg	8.5	50 (4.1 ± 0.1)	41 (3.3)	9
Cu/ZnO:Ga	10.8	86 (7.0 ± 0.1)	64 (5.3)	22
Cu/ZnO:Al	9.3	73 (5.9 ± 0.1)	54 (4.4)	19

[a]Determined from XRF measurements. [b]Metallic Cu surface area assuming a stoichiometric reaction of N_2O with Cu surface atoms. [c]Number of sites of reaction of H_2 with Cu_2O surface atoms after oxidation of Cu surface with N_2O.

different uptakes of physisorbed humidity and CO_2 of the supports, leading to weighing errors during catalyst preparation. The N_2O-chemisorption capacity, measured by the N_2O-RFC method,[12] was between 50 and 85 $\mu mol\,g^{-1}$ (corresponding to apparent Cu-SA_{N_2O} values of 4–7 $m^2\,g^{-1}$) for the different samples (see Table 2). Due to the sensitivity of the measurement, the error of the N_2O-RFC method is usually estimated around 1 $m^2\,g^{-1}$, but repeated measurements of the same samples showed a much smaller error, below 5%, for the investigated samples. Different loadings from 5 to 15% Cu on the unpromoted sample showed that the N_2O capacity scales linearly with the amount of Cu within the uncertainty of the measurement, thus indicating that the impregnation was not limited by the available support SA within the loading regime studied here.

As the N_2O-RFC method probes not only the Cu surface atoms but also redox-active defect sites of the ZnO support,[13,24] the Cu-SA was measured with a method called H_2-transient adsorption (TA).[13] The number of sites measured by H_2-TA were all smaller than those measured by N_2O-RFC, with values between 40 and 65 $\mu mol\,g^{-1}$, corresponding to surface areas of 3.3 $m^2\,g^{-1}$ for Cu/ZnO:Mg and 5.3 $m^2\,g^{-1}$ for Cu/ZnO:Ga. The theoretical maximum Cu-SA value, which can be expected for samples with measured loadings of 8.5–10.8% Cu and a particle size of about 10 nm (see below), is 5.7–7.3 $m^2\,g^{-1}$, which leads to the reasonable assumption that the interface ratio of the particles is between 27 and 42%. From the difference in the two measurement methods the number of oxidizable defects at the surface of ZnO can be calculated. The highest values of 22 $\mu mol\,g^{-1}$ were found for the Cu/ZnO:Ga sample, similar to the case for Cu/ZnO:Al and Cu/ZnO. For Cu/ZnO:Mg this number was much lower, with only 9 $\mu mol\,g^{-1}$ indicating a different impact of the Mg^{2+} promoter on the properties of the ZnO component as shown below (Table 2).

SEM gave further insights into the microstructure of the samples (see Figure 2). The ZnO prepared by the precipitation of a hydrozincite precursor exhibited a platelet-like and porous morphology, assembling into spherical aggregates. Al promotion did not influence the morphology drastically. However, the platelets appeared thinner, rendering a more sheetlike occurrence. Impregnation with Cu and recalcination changed

the morphology (see Figure 2e,f) toward more granular particles. For Al-promoted samples, the platelet morphology seemed to be less altered by this step. The morphology of ZnO as well as Cu/ZnO does not seem to be significantly altered after reduction at 523 K, as was shown by SEM of the reduced samples (see Figure S5 in the Supporting Information).

The reduced samples Cu/ZnO and Cu/ZnO:Al have been further investigated with HAADF-STEM (see Figure 3 and Figure S3 in the Supporting Information). The images reveal that the Cu nanoparticles (<10 nm, red) are dispersed on highly porous ZnO (yellow) supports.

With diffuse reflectance UV−vis spectroscopy optical band gaps of the supports were estimated. It was found that Mg^{2+} increased the apparent optical band gap of ZnO, whereas Al^{3+} and Ga^{3+} led to a decrease of the optical band gap (see Figure 4 and Table 3). This is in agreement with the observed color of the samples. ZnO:Mg was lightest in color, whereas ZnO:Ga and ZnO:Al were deeper yellow. This can be interpreted as the formation of defect states by Ga^{3+} and Al^{3+} in the band gap as is expected for trivalent dopants in n-type semiconductors, while Mg^{2+} makes ZnO more insulating. Additionally, the shape of the absorption profile around the band edge is different for ZnO and the differently promoted ZnO:Al and ZnO:Ga samples. This may also indicate that Al and Ga promoters occupy different local geometries, which may lead to different positions of the donor states within the band gap. When the sample was heated under inert gas to 503 K, the band gap decreased by 70−120 meV. This is a result of two effects: (i) expansion of the lattice parameters, and (ii) the thermal excitation of electrons and holes (to about 35 meV).[16] A change in the atmosphere at 503 K, either reducing or oxidizing, did not alter the optical band gap significantly at the temperature and time scale studied.

Temperature-programmed reduction (TPR) was performed to give further insight into the reducibility of the system. Pure bulk ZnO is only reduced at temperatures above 700 K.[25] In our study we only investigated the temperature range up to 623 K, as this is the range relevant for the studied reactions and will give information about defect formation such as oxygen vacancies. The pure supports showed a very weak reduction signal, in agreement with the expected relatively small amount of defect formation in comparison to complete bulk reduction (see Figure 5a). Undoped ZnO started to reduce at the lowest temperature, whereas ZnO:Mg showed the weakest reduction signal at the highest temperatures. A relatively strong reduction signal around 460 K was present for ZnO and ZnO:Ga. This might be attributed to the reduction of special oxygen defects in the ZnO lattice, as suggested by correlation with EPR results (see below).

The profiles of the impregnated samples showed the successful deposition of nanocrystalline CuO, which was reduced at temperatures between 480 and 500 K depending on the support (see Figure 5b). These values agree well with reduction peak maxima reported for other systems with nanocrystalline CuO particles.[26] All peaks featured a strong shoulder at the low-temperature side of the main peak. A similar shape was observed for the reduction of Cu catalysts derived from a Cu,Zn,Al-layered double hydroxide (LDH) precursor.[27] The shoulder of this ex-LDH catalyst was assigned to the first step of the reduction Cu(II) → Cu(I) → Cu(0) and was caused by a strong interaction of Cu and the oxide matrix, which kinetically stabilizes the Cu(I) intermediate.[27] A similar effect was seen here, which indicates a strong interaction between the Cu species and the ZnO:M supports. A strong interaction between support and Cu component was also confirmed by the nonadditive behavior of
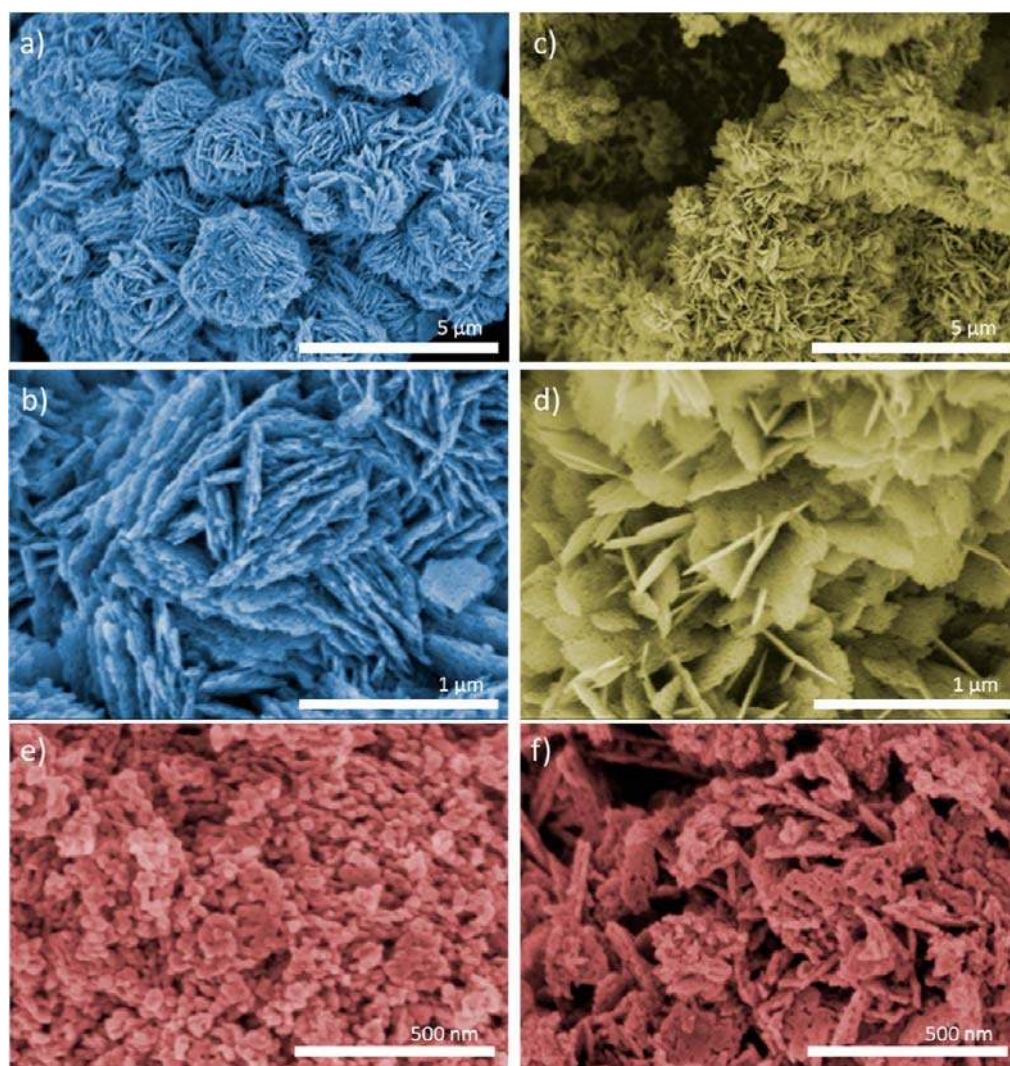
Figure 2. SEM images of ZnO:M supports ((a, b) ZnO and (c, d) ZnO:Al) and of impregnated samples ((e) CuO/ZnO and (f) CuO/ZnO:Al). The original, uncolorized images are shown in the Supporting Information.

the reduction signals. The broad reduction signals of the support around 550 K have vanished in the impregnated samples (see Figure 5c). Furthermore, the much stronger contribution of the Cu component to the reduction profile was significantly influenced by the promoter in the support, which also requires a strong interaction. The reduction onset temperature was lower for CuO than for any of the ZnO:M supports, as can be expected for the much more precious element Cu. Already the onset temperature of the CuO reduction was influenced by the promoter species. CuO/ZnO started to reduce first, around 400 K, and the promoted CuO/ZnO:M (M = Al, Ga, Mg) samples only started slightly later to reduce. Additionally, the main reduction peak shifted from 480 K toward higher temperatures by 10−20 K in the order Ga < Al < Mg, as can be seen in the difference plots (Figure 5d). The medium shift of Al- and Ga-promoted CuO/ZnO:M might be explained by the formation of a more extended ZnO overlayer, in comparison to the unpromoted sample, or an additional stabilization of the intermediate Cu(I) species by the SMSI, which might slow the hydrogen consumption slightly. The higher temperature of the main reduction peak of CuO/ZnO:Al in comparison to that of

the Ga-promoted samples implies a stronger SMSI for the former. The reason for the strong shift of the reduction profile of CuO/ZnO:Mg is not as easy to understand. An explanation might be a lower hydrogen spillover effect, which might compensate for the weaker metal−support interaction. Quantification of the reduction signals under the assumption that only CuO was contributing to the hydrogen consumption yielded amounts between 10.7 and 14.1 wt % of CuO. All samples showed H_2 consumption higher than what would be expected from the XRF results, if only CuO contributed to the reduction signal. The contribution of the partial reduction of ZnO to ZnO_{1-x} was higher for the impregnated CuO/ZnO:M than for the pure ZnO:M supports. A strong increase in the bulk reducibility of ZnO in the vicinity of Cu was observed, except for the Mg-doped sample. Especially Al^{3+} seems to promote the oxygen vacancy formation in ZnO (see Table 4). These results for the bulk confirm the trend of the oxygen vacancies at the surface obtained from the different Cu-SA measurements earlier (Table 2). It becomes evident that the promoter species influence both reduction processes: CuO → Cu and ZnO → ZnO_{1-x}. Furthermore, the presence of Cu influences the
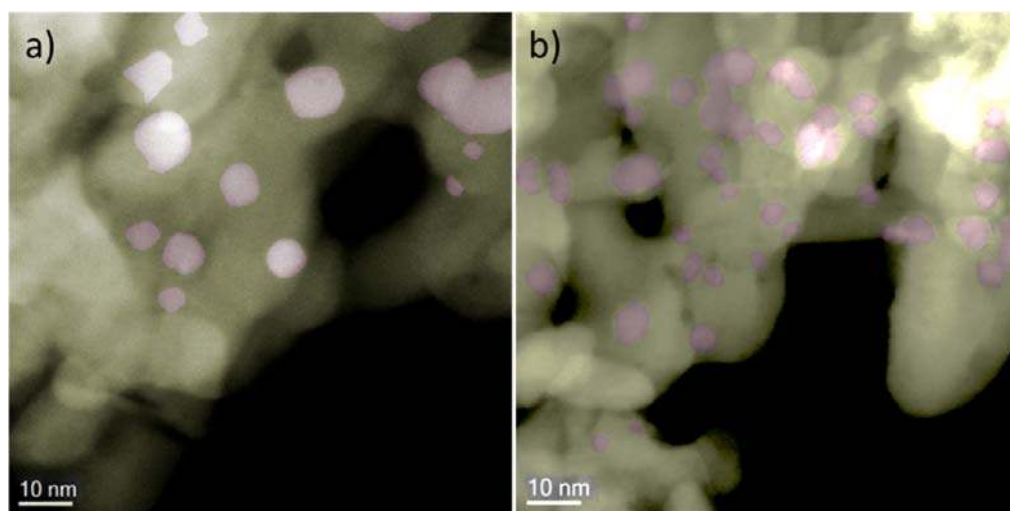
Figure 3. STEM micrographs of (a) Cu/ZnO and (b) Cu/ZnO:Al. Within the images ZnO moieties are highlighted in yellow, whereas Cu particles are presented in red. The original images are given in the Supporting Information.
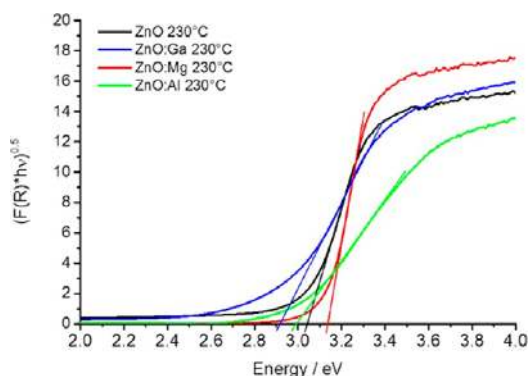

Figure 4. Tauc plot for band gap estimation from UV−vis spectra.

Table 3. Band Gap Energies

	optical band gap[a] (eV)	
	room temp	503 K
ZnO	3.12 ± 0.12	3.03 ± 0.05
ZnO:Mg	3.20 ± 0.08	3.13 ± 0.05
ZnO:Al	3.07 ± 0.04	2.99 ± 0.02
ZnO:Ga	3.03 ± 0.05	2.91 ± 0.04

[a]Errors are determined from uncertainty of linear fit.

reduction of $ZnO \rightarrow ZnO_{1-x}$ and facilitates the formation of oxygen vacancies, by shifting it to lower temperatures and increasing the extent of vacancy formation. This phenomenon can probably be related to the SMSI effect, the formation of a ZnO overlayer on Cu, which is assumed to strongly facilitate the oxygen vacancy formation due to the driving force toward surface brass formation.

Electronic Properties. Using a contactless conductivity measurement technique based on the microwave cavity perturbation technique,[17a] the conductivity of the supports in inert (N_2), reducing (5.2 vol % of H_2 in N_2), and oxidizing (5.2 vol % of O_2 in N_2) gas environments was measured at 503 K. The experiments were performed to identify the effect of the different dopant ions on (1) the absolute conductivity and (2) the redox response of ZnO at the catalytically relevant temperature of 503

K. The results summarized in Figure 6 show that the conductivity behavior is strongly modified by the different dopants. The initial conductivity decrease for all samples during the first temperature ramp from room temperature to 503 K is unexpected for semiconductors but could be explained by the desorption of residual water in the samples that gives also rise to a strong microwave absorption signal overlapping the original conductivity of ZnO. The decreasing conductivity during the final ramp from 503 K to room temperature shows indeed the expected temperature behavior of a semiconductor. ZnO is typically an n-type semiconductor with electrons as majority charge carriers, which explains the increasing conductivity in H_2 due to the donation of electrons into the material upon chemisorption or reaction. Interestingly, the conductivity of ZnO decreases already during the subsequent treatment in N_2, probably pointing to a rather weak adsorption of H_2 already desorbing in flowing N_2. The effect of O_2 is very small, leading only to a weak consumption of conduction electrons. The redox cycle is reversible, as indicated by the repeated treatment in H_2 and O_2, though the conductivity increase is even more pronounced after the second H_2 treatment.

In ZnO:Al the conductivity rises by several orders of magnitude in comparison to pure ZnO. The introduction of Ga induces an even higher absolute conductivity value. Both samples show as well an increasing conductivity in H_2 but, in contrast to ZnO, exhibit also a decreased charge transport in O_2. The conductivities relax already in N_2 to the original values measured in inert gas, though the kinetics are significantly slower than those in ZnO, suggesting a stronger adsorption of the gases in the doped materials. A completely different behavior is observed for ZnO:Mg. Mg^{2+} leads to both a decrease of the absolute value of the conductivity and a totally extinguished redox response in H_2 and O_2.

The effect of the dopants resembles very well the modification of the apparent band gap observed in the UV−vis spectroscopy experiments. Al and Ga with a preferred oxidation state of 3+ substituting Zn^{2+} in the crystal lattice are n-type dopants that create shallow donor states in the band gap of ZnO, inducing a higher density of free charge carriers in the conduction band. The formation of additional donor states in the band gap is supported by the observation of a decreased optical band gap. These donor
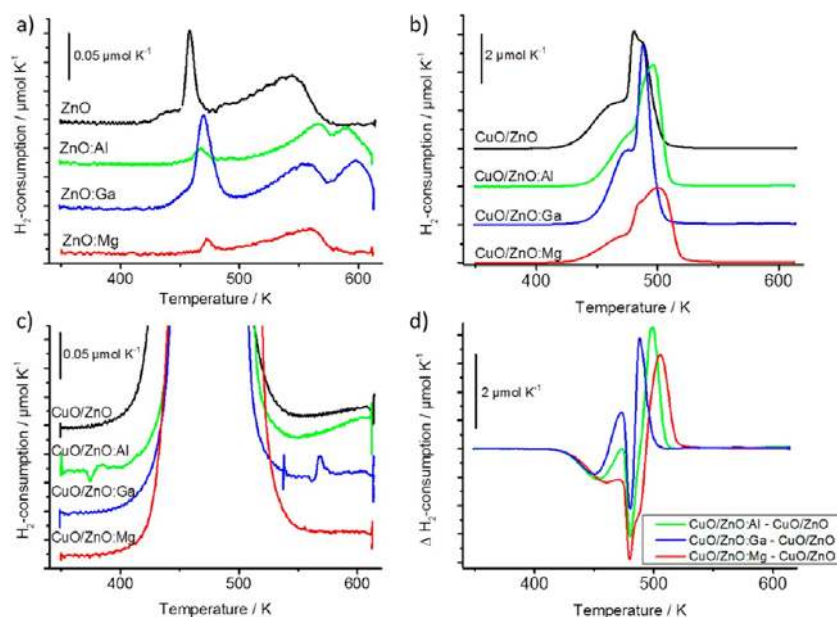
Figure 5. TPR profiles of (a) pure supports and (b) impregnated CuO/ZnO:M supports. (c) Detailed section of the profiles of CuO/ZnO:M. (d) Difference plots of the promoted samples CuO/ZnO:M relative to the unpromoted CuO/ZnO.

Table 4. TPR Results

	H$_2$ consumption pure support (μmol g^{-1})	reducible species pure support (%) (up to 623 K)	calcd amt of CuO (values from XRF) (wt %)	T$_{max}$ (K)	amt of reducible support species[a] (μmol g^{-1})
ZnO	46	0.4	12.7 (11.5)	480	151
ZnO:Mg	22	0.2	10.7 (10.4)	500	38
ZnO:Ga	74	0.6	14.1 (13.2)	488	113
ZnO:Al	37	0.3	13.0 (11.4)	496	201

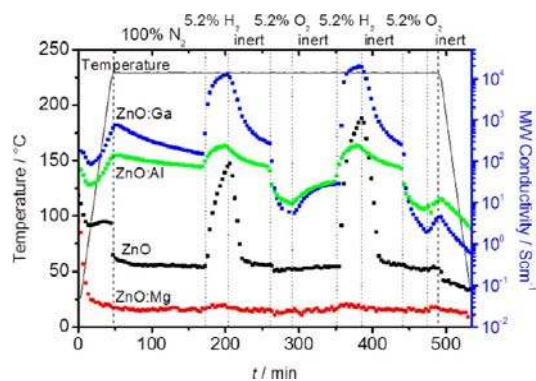[a]Calculated from difference of TPR and XRF CuO quantification.

Figure 6. Microwave conductivity measurements of ZnO supports in different gas atmospheres at elevated temperatures.

states not only increase the absolute conductivity but can also strongly interact with H$_2$ and in particular with O$_2$, leading to an increased charge transfer with adsorbed molecules and hence to a stronger gas-phase response of the conductivity. In contrast, Mg^{2+} apparently reduces the density of donor states significantly, as also indicated by the increased optical band gap, and hence decreases the absolute conductivity and quenches the interaction with H$_2$ and O$_2$. These findings indicate that the introduced dopants are strong electronic promoters for semiconducting ZnO.

The interpretation that shallow donor states are formed by doping ZnO with Ga and Al is supported by EPR measurements. Figure 7 clearly shows strong resonances at g values of 1.963 for Al- and Ga-doped ZnO, which are attributed to shallow donor centers, typically ionized impurities[28] or zinc interstitials,[29] as might be additionally induced by the Al^{3+} and Ga^{3+} dopants to
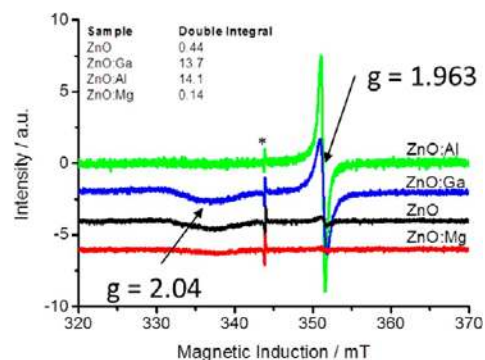

Figure 7. EPR measurements of the samples at 293 K under ambient conditions. Spectra of the differently promoted ZnO samples have been offset by a constant value for better visibility. The sharp signal at a magnetic induction of about 344 mT (g factor 1.9796) marked with an asterisk is from an external Cr^{3+}/MgO standard introduced into the resonator in order to normalize the intensity of the spectra to the maximum of this signal.

compensate for the charge mismatch. The pure ZnO and Mg-doped ZnO show only a very small resonance signal at this position, supporting the much lower concentration of shallow donor states in these systems. A direct quantitative comparison is possible on the basis of the double integral values of the signal depicted in the inset of Figure 7.

There is a second, very broad resonance signal at lower magnetic field strength with a g factor of around 2.04 for ZnO and ZnO:Ga, which is close to the value reported for single electrons trapped in oxygen vacancies.[28] Other studies report that a very broad feature between g values of 2.01 and 2.05 is the result of chemisorbed oxygen at the ZnO surface.[29,30] Interestingly, this low-field resonance coincides with the occurrence of a (relatively) strong low-temperature reduction peak for the same two samples (compare with Figure 5a). This could indicate that these defects are easily reducible species. Al^{3+} and Mg^{2+} doping leads to a strong decrease of this low-temperature reduction peak and of the EPR resonance signal around 2.04. This might then correspond to fewer oxygen defects present in ZnO:Al and ZnO:Mg. Likely, the "hardness" of the smaller and highly charged cations Al^{3+} and Mg^{2+} leads to a stronger binding of lattice oxygen and thus prevents the formation of oxygen vacancies.[31] The different behaviors of Al^{3+} and Ga^{3+} dopants, despite their similar valence electron configurations, could be explained by the difference in polarizability and ionic radii of the dopants, properties in which Ga^{3+} is much more similar to Zn^{2+} in comparison to Al^{3+}. Another reason can be the different occupations of the lattice sites in the wurtzite structure. The two different sites, which can be occupied by the Al or Ga dopants, are substitutional sites with tetrahedral symmetry and interstitial sites with octahedral symmetry. For Al^{3+} it was shown by NMR that for small concentrations the tetrahedral sites are occupied.[9] Ga^{3+}, on the other hand, could be expected to preferentially occupy octahedral sites due to its larger ionic radius.[21,31] This is also supported by the analysis of the ZnO lattice parameters obtained by XRD.[21] Rietveld analysis revealed a higher unit cell volume for ZnO:Ga and a slightly smaller volume for ZnO:Al (see Table S1 in the Supporting Information), supporting the assumption that Al^{3+} occupies substitutional sites and Ga^{3+} preferentially octahedral interstitials. It is noted that there are also studies reporting the opposite behavior,[32] but here the aforementioned assignment is also supported by other properties that are different for the two materials, such as conductivity behavior, band gap shift relative to the undoped material, and ZnO lattice parameters. It seems these properties depend on the mode of preparation.

Surface Characterization. Depth profiles of the catalyst surface of the three samples Cu/ZnO, Cu/ZnO:Mg, and Cu/ZnO:Ga have been recorded by XPS after prereduction and inert transfer into the measurement cell (see Figure 8). Significant deviation of the surface composition from the nominal composition is observed for all three measured samples. The Cu amount is enriched due to the mode of preparation (impregnation), yielding small Cu nanoparticles at the surface of the ZnO support. Different behavior is observed for the dopant. The Mg content is constant at 2−3% and corresponds to the nominal value. However, the Ga content is strongly increased for the most surface sensitive measurement (8%) and decreases for more bulklike measurements with higher excitation energy to 0. This behavior agrees very well with the behavior reported previously for ZnO:Al, that upon reduction an enrichment of Al^{3+} toward the surface takes place.[9]
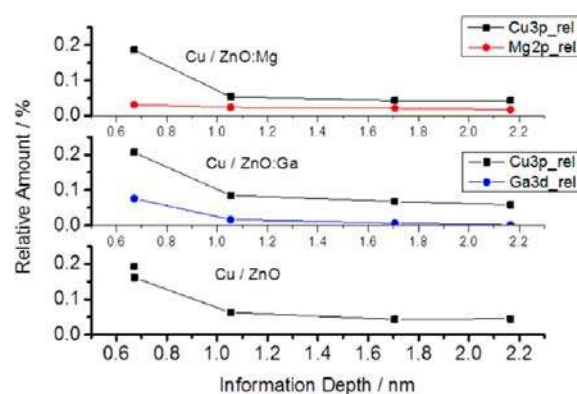

Figure 8. Surface compositions with depth profiles as determined by XPS.

Activity in rWGS and MeOH Synthesis. The activity of the catalysts has been tested in the reverse water-gas shift (rWGS) reaction at ambient pressure as well as in methanol synthesis at 30 bar. In both reactions the trend regarding the activities was the same for the sample series: the Mg-doped catalyst showed the least activity, followed by the undoped catalyst, and the highest activity was shown by the Al- and Ga-doped catalysts. This observation agrees well with the conductivity measurements of the supports, indicating that the different electronic properties of ZnO as induced by the dopants affect the catalytic properties of the Cu/ZnO:M catalysts.

The rWGS reaction was performed using two different H_2/CO_2 ratios and setups. With the stoichiometric $1/1$ H_2/CO_2 feed ratio, activities for CO formation of $21-31$ $\mu mol/(min\ g_{cat})$ were measured at 503 K for the differently promoted samples. By normalization of the activity per Cu-SA_{N_2O}, measured by N_2O chemisorption, a so-called intrinsic activity was calculated (see Figure 9). In this reaction, in addition to the unpromoted ZnO
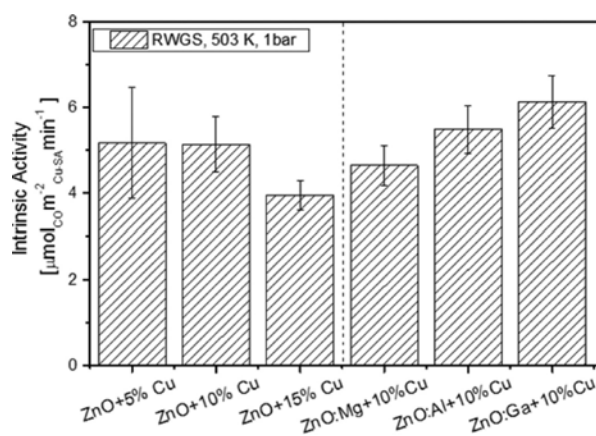

Figure 9. Intrinsic activity in rWGS reaction.

samples impregnated with 10% Cu, two samples with 5% and 15% Cu were tested. The 5% and 10% samples showed a linear increase in activity and Cu-SA with respect to the copper loading, and therefore they had the same intrinsic activity for rWGS. This indicates a homogeneous particle distribution. A 15% copper sample already led to intrinsically less active catalyst particles (see Figure 9), which is why a 10% Cu loading was used for comparison of the different supports. Activation energies for CO

formation in rWGS were smaller for the more active Al- and Ga-doped samples (87 and 89 kJ/mol, respectively) and higher for the Mg-doped and unpromoted samples: 98 and 99 kJ/mol, respectively. This indicates that the trivalent promoters in the support have a positive effect on the nature of rWGS sites, while Mg did not show a positive or negative effect in this reaction.

The reaction order in H_2 was 0.2, and in CO_2 it was 0.2−0.3 for the tested catalysts (see Table 5), which is of the same magnitude

Table 5. Reaction Orders of H_2 and CO_2 in rWGS with a H_2/CO_2 Ratio in the Range of 0.33−3 at 503 K

	reaction order	
	H_2	CO_2
Cu/ZnO	0.18	0.2
Cu/ZnO:Mg	0.18	0.2
Cu/ZnO:Al	0.15	0.3
Cu/ZnO:Ga	0.16	0.3

of reaction orders reported earlier for Cu-based catalysts in rWGS.[33] In the study by Ginés et al.[33] two different regimes were identified. With excess H_2 ($H_2/CO_2 > 3$) the reaction order in hydrogen is negligible, but the reaction order in CO_2 is about 1.1. Under less hydrogen rich conditions, the order in CO_2 is smaller, about 0.3, and the reaction order in H_2 is 0.8. With the testing conditions used in this study ($0.3 < H_2/CO_2 < 3$), we were in the transition between both regimes, which is why the reaction order of H_2 matches with the hydrogen-rich conditions but for CO_2 it is closer to CO_2-rich conditions. Furthermore, the reaction orders seemed to be influenced by the promoters: whereas the reaction order of H_2 decreased slightly upon promotion with the trivalent cations Al^{3+} and Ga^{3+}, the reaction order in CO_2 increased. The change in activation energy and the slight trend in the reaction order of H_2 agrees well with the commonly assumed surface redox mechanism for the rWGS,[34] except for the suggestion that clean metallic Cu is regarded as the active phase. The observed facilitated reducibility and the stronger adsorption of H_2 on the Al^{3+}- and Ga^{3+}-doped supports might indicate an active role of ZnO in the rWGS mechanism or an alteration of the electronic states of the Cu surface by SMSI. Traces of methanol have been detected by GC under these reaction conditions, but they were below the quantification limit.

In the hydrogen-rich feed gas composition ($H_2/CO_2 = 3/1$) at ambient pressure methanol could already be quantified in the product stream. The activation energies in methanol synthesis for the more active Cu/ZnO:Ga, Cu/ZnO:Al, and Cu/ZnO were determined to be 37−41 kJ/mol, and an activation energy of 50 kJ/mol was found for Cu/ZnO:Mg, showing a detrimental effect of Mg doping for methanol synthesis. Under these conditions, activation energies for rWGS are higher and show less difference: 112 kJ/mol for Ga- and Al-promoted catalysts and 115 kJ/mol for the Mg-doped and undoped sample (see Table 6).

The order in the activity of methanol synthesis at 30 bar from a typical syngas mixture with a $CO_2/CO/H_2$ composition of 8/6/59 was the same as that for the rWGS reaction: Cu/ZnO:Mg was the least active, followed closely by Cu/ZnO. Cu/ZnO:Al and Cu/ZnO:Ga were nearly twice as active (see Figure 10a). The catalysts were quite stable over 8 h time on stream. Only Cu/ZnO:Al showed an activation behavior ("induction period") and reached steady state after 2 h. The intrinsic activity calculated by normalizing the activity to the N_2O chemisorption capacity showed smaller differences between the different samples than for rWGS (Figure 10b). Cu/ZnO:Al was slightly more active

Table 6. Activation Energies in rWGS and Methanol Synthesis from Different Feed Gases

	RWGS CO formation[a] (kJ mol⁻¹)		MeOH formation (kJ mol⁻¹)	
	$H_2/CO_2 = 1/1$[a]	$H_2/CO_2 = 3/1$[b]	$H_2/CO_2 = 3/1$; 1 bar[c]	syngas; 30 bar[b]
Cu/ZnO	99	115	41	53
Cu/ZnO:Al	87	112	40	56
Cu/ZnO:Ga	89	112	37	57
Cu/ZnO:Mg	98	115	50	56

[a]T = 483−503 K. [b]T = 463−523 K. [c]T = 463−503 K.

than the other samples, but the differences were small. Only when the activity was normalized to the "only Cu surface sites" determined by H_2-TA were the differences small but significant. Cu/ZnO:Al had the highest intrinsic activity, closely followed by Cu/ZnO:Ga. The Mg-doped and unpromoted samples had lower intrinsic activities.

The apparent activation energies in this reaction are nearly the same for all the samples at approximately 56 kJ mol⁻¹. This value matches very well with the recently published activation energy of 57 kJ mol⁻¹ for a high surface area reference-type catalyst (FHI-std) tested in our laboratory under the same conditions.[26b] This indicates the comparability of the active sites of these model-type catalysts prepared by impregnation with industrially relevant systems prepared by coprecipitation.

For both reactions□ methanol synthesis and rWGS□ a dependence of the activity on the promoted support was found. In the rWGS reaction that was tested under mild conditions at ambient pressure and low reduction potential, Al^{3+} and Ga^{3+} seem to work as electronic promoters. The activation energy is lowered and the reaction order in hydrogen is slightly decreased. At the same time the intrinsic activity increased. This could be explained by a facilitation of the reducibility of the ZnO support and the introduction of shallow donor states as reflected in a change in the optical band gap. This might lead to a stronger adsorption of H_2, as was also shown by the conductivity measurements. A change in the chemical potential at the Cu−support interface could thus influence the activity of the active Cu phase. Although in the commonly assumed surface redox mechanism for the rWGS usually the CO_2 dissociation is regarded as the rate-determining step,[33,35] it is plausible to assume a beneficial effect also for the facilitation of the hydrogen adsorption, especially under the hydrogen-lean conditions used (in comparison to the usually hydrogen rich conditions used for CO_2 hydrogenation to methanol, where rWGS is regarded as a side reaction).

In methanol synthesis, under much more strongly reducing conditions of 30 bar and high H_2 + CO content, the negligible difference in the activation energy between the differently promoted catalysts indicates that the electronic effect of the dopants on the ZnO does not significantly affect the energetic state of the active site of the rate-determining step(s). The significant differences in intrinsic activity normalized by H_2-TA sites nevertheless point to a significant promoter effect, which must then be a structural effect. Interestingly, when it was normalized to the N_2O capacity, the intrinsic activity only showed a much weaker effect of the promoter. It seems that, when differently promoted catalysts with otherwise similar preparation histories are compared, the N_2O chemisorption capacity scales nicely with the activity, in agreement with previous reports from the literature. Apparently, as the
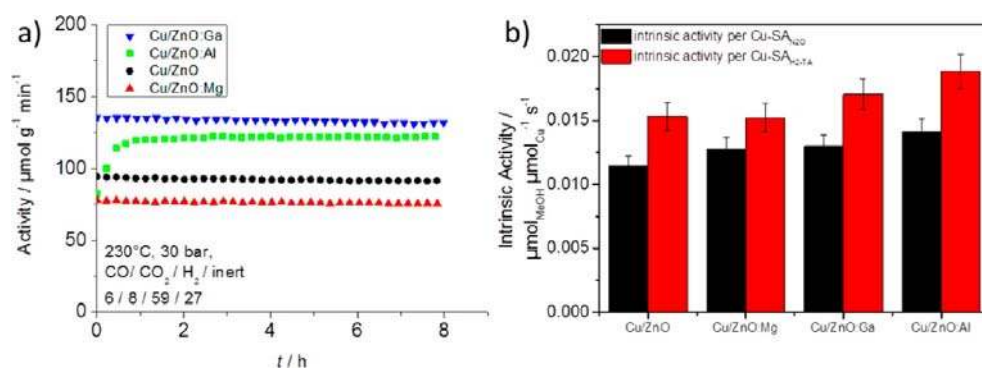
Figure 10. Activity of Cu/ZnO:M catalysts in methanol synthesis: (a) weight time yield; (b) intrinsic activity with respect to differently quantified Cu sites.

differences between the differently promoted catalysts in N_2O-normalized intrinsic activities were smaller, the defect sites that are probed by N_2O-RFC in addition to the Cu sites are linked to the activity. This can also explain the effect seen for promoted Cu/ZnO:Al catalysts prepared by coprecipitation of zincian malachite, where the intrinsic activity (normalized by the N_2O capacity) decreases in comparison to the binary Cu/ZnO catalyst.[8] On the other hand, as shown in ref 36, if for example the calcination temperature is varied, the absolute number of ZnO defect sites was not linked to the intrinsic activities.

The redox-active defect sites, as also introduced by the promoter, seem to be linked to the reducibility of the ZnO and can be interpreted as a measure for the SMSI. The higher mobility of the ZnO on the surface of Cu leads to a higher number of active sites for methanol synthesis and a greater Cu–ZnO interface, which would explain the structural promoter effect seen for Al^{3+}- and Ga^{3+}-doped Cu/ZnO catalysts. The XPS data do not support an increased presence of Zn on the surface for the Cu/ZnO:Ga sample in comparison to the unpromoted and Cu/ZnO:Mg samples. However, this might be due to the fact that the XPS measurements were not performed under high-pressure in situ conditions, where the mobility of ZnO could be more effective. A pressure-dependent change of the active site is also supported by the observation that the activation energy for methanol is approximately 10 kJ/mol lower at ambient pressure in comparison to the conditions at 30 bar and additionally depends on the promoter.

Charge transfer between the semiconductor and the metal was already suggested by Frost et al. as the formation of a Schottky junction and proposed as the origin of the Cu–ZnO synergy.[37] This charge transfer might be significantly influenced by band bending through defect states at the surface and could explain the promoting effect of Al^{3+} and Ga^{3+} dopants in a way similar to that described above for the rWGS reaction.

CONCLUSION

We successfully prepared Cu/ZnO catalysts in a two-step procedure, which allowed us to study the effect of different promoters on the oxide support independently from the active metal part. Insights into the electronic structure of ZnO as a catalyst support and the influence of different dopants were provided by contactless conductivity measurements, EPR and UV–vis spectroscopy, and TPR measurements. Surface-sensitive measurements of the impregnated catalysts yielded additional information on the active state. Comparison of the character-ization data of the supports with the results from the activity measurements revealed parallel trends with respect to the dopants. While the trivalent promoters Al^{3+} and Ga^{3+} improve conductivity and increase the defect level in the support, the Mg^{2+} promoter decreases the conductivity of the ZnO support. The catalytic data show that although the active phase is metallic copper, the promoted ZnO significantly influences the activity. The rWGS activity data suggest that Al^{3+} and Ga^{3+} act as electronic promoters in the ZnO, lowering the activation energy and facilitating the H_2 activation. Mg^{2+}, on the other hand, has no beneficial influence on the activity. The small differences in the activation energy in methanol synthesis at 30 bar indicate that Al^{3+} and Ga^{3+} either do not influence the rate-determining step of methanol synthesis or rather act as structural promoters for this reaction. Due to the highly reducing reaction conditions during methanol synthesis, a facilitated reducibility of ZnO seems not that important in comparison to less reducing reaction conditions with more CO_2. Although we assume that the different promoters stay in the lattice of the ZnO support, it might also be possible that the promoters migrate into the Cu component under reaction conditions and affect the activity from there. The mobility and resulting surface enrichment of the Al^{3+} and Ga^{3+} promoters under reducing conditions were shown by XPS depth profiling. We have shown that the SMSI can be tuned by the use of suitable cations to promote structurally and/or electronically the active site for rWGS and methanol synthesis.

■ ASSOCIATED CONTENT

Ⓢ Supporting Information

The following file is available free of charge on the ACS Publications website at DOI: 10.1021/acscatal.5b00188.

Additional characterization data and a list with the sample numbers for future reference (PDF)

■ AUTHOR INFORMATION

Corresponding Authors

*E-mail for M.E.: me@fhi-berlin.mpg.de.
*E-mail for M.B.: malte.behrens@uni-due.de.

Present Addresses

[†](N.T.) Nirmalagiri College, Nirmalagiri, Kannur, Kerala, India.
[‡](Á.G.) Instituto de Catálisis y Petroleoquímica (CSIC), C/ Marie Curie 2, 28049 Cantoblanco, Madrid, Spain.
[§](R.S.) Department of Heterogeneous Reactions, Max-Planck-Institut für Chemische Energiekonversion, Stiftstrasse 34-36, 45470 Mülheim an der Ruhr, Germany.

‖(M.B.) University of Duisburg-Essen, Faculty of Chemistry and Center for Nanointegration Duisburg-Essen (CENIDE), Universitätstrasse 7, 45141 Essen, Germany.

Notes

The authors declare no competing financial interest.

■ REFERENCES

(1) (a) Behrens, M.; Studt, F.; Kasatkin, I.; Kühl, S.; Hävecker, M.; Abild-Pedersen, F.; Zander, S.; Girgsdies, F.; Kurr, P.; Kniep, B. L.; Tovar, M.; Fischer, R. W.; Norskov, J. K.; Schlögl, R. *Science* **2012**, *336*, 893−897. (b) Spencer, M. S. *Top. Catal.* **1999**, *8*, 259−266. (c) Grunwaldt, J. D.; Molenbroek, A. M.; Topsøe, N. Y.; Topsøe, H.; Clausen, B. S. *J. Catal.* **2000**, *194*, 452−460.

(2) Choi, Y.; Futagami, K.; Fujitani, T.; Nakamura, J. *Appl. Catal., A* **2001**, *208*, 163−167.

(3) (a) Burch, R.; Golunski, S. E.; Spencer, M. S. *J. Chem. Soc., Faraday Trans.* **1990**, *86*, 2683. (b) Spencer, M. *Catal. Lett.* **1998**, *50*, 37−40.

(4) (a) Topsøe, N.-Y.; Topsøe, H. *Top. Catal.* **1999**, *8*, 267−270. (b) Naumann d'Alnoncourt, R.; Xia, X.; Strunk, J.; Loffler, E.; Hinrichsen, O.; Muhler, M. *Phys. Chem. Chem. Phys.* **2006**, *8*, 1525−1538.

(5) (a) Schott, V.; Oberhofer, H.; Birkner, A.; Xu, M.; Wang, Y.; Muhler, M.; Reuter, K.; Wöll, C. *Angew. Chem., Int. Ed.* **2013**, *52*, 11925−11929. (b) Kanai, Y.; Watanabe, T.; Fujitani, T.; Saito, M.; Nakamura, J.; Uchijima, T. *Catal. Lett.* **1994**, *27*, 67−78.

(6) Koel, B. E.; Kim, J. Promoters and Poisons. In *Handbook of Heterogenous Catalysis*; Ertl, G., Knözinger, H., Schüth, F., Weitkamp, J., Eds.; Wiley-VCH: Weinheim, Germany, 2008; p 1593.

(7) Hansen, J. B.; Nielsen, P. E. H., Methanol Synthesis. In *Handbook of Heterogeneous Catalysis*; Ertl, G., Knözinger, H., Schüth, F., Weitkamp, J., Eds.; Wiley-VCH: Weinheim, Germany, 2008; p 2920.

(8) Behrens, M.; Schlögl, R. *Z. Anorg. Allg. Chem.* **2013**, *639*, 2683−2695.

(9) Behrens, M.; Lolli, G.; Muratova, N.; Kasatkin, I.; Hävecker, M.; d'Alnoncourt, R. N.; Storcheva, O.; Köhler, K.; Muhler, M.; Schlögl, R. *Phys. Chem. Chem. Phys.* **2013**, *15*, 1374−1381.

(10) Özgür, Ü. A. Y.; Liu, C.; Teke, A.; Reshchikov, M.; Dogan, S.; Avrutin, V.; Cho, S.; Morkoc, H. *J. Appl. Phys.* **2005**, *98*, 041301.

(11) Coelho, A. A., *TOPAS: General Profile and Structure Analysis Software for Powder Diffraction Data, Version 3.0*; Bruker AXS, Karlsruhe, Germany, 2006.

(12) Chinchen, G. C.; Hay, C. M.; Vandervell, H. D.; Waugh, K. C. *J. Catal.* **1987**, *103*, 79−86.

(13) Kuld, S.; Conradsen, C.; Moses, P. G.; Chorkendorff, I.; Sehested, J. *Angew. Chem., Int. Ed.* **2014**, *53*, 5941−5945.

(14) Weber, R. S. *J. Catal.* **1995**, *151*, 470−474.

(15) (a) Khodakov, A.; Olthof, B.; Bell, A.; Iglesia, E. *J. Catal.* **1999**, *181*, 205. (b) Chen, K.; Bell, A. T.; Iglesia, E. *J. Catal.* **2002**, *209*, 35−42. (c) Barton, D. G.; Shtein, M.; Wilson, R. D.; S.L, S.; Iglesia, E. *J. Phys. Chem. B* **1999**, *103*, 630.

(16) Smith, R. A. *Semiconductors*, 2nd ed.; Cambridge University Press: Cambridge, U.K., 1978.

(17) (a) Eichelbaum, M.; Stoßer, R.; Karpov, A.; Dobner, C.-K.; Rosowski, F.; Trunschke, A.; Schlogl, R. *Phys. Chem. Chem. Phys.* **2012**, *14*, 1302−1312. (b) Heine, C.; Girgsdies, F.; Trunschke, A.; Schlögl, R.; Eichelbaum, M. *Appl. Phys. A: Mater. Sci. Process.* **2013**, *112*, 289−196.

(18) Shannon, R. *Acta Crystallogr., Sect. A: Cryst. Phys., Diffr., Theor. Gen. Crystallogr.* **1976**, *A 32*, 751−767.

(19) (a) Chen, Z.; Zhan, G.; Lu, Z. *J. Mater. Sci.: Mater. Electron.* **2014**, *25*, 1724−1730. (b) Zamiri, R.; Singh, B.; Scott Belsley, M.; Ferreira, J. *Ceram. Int.* **2014**, *40*, 6031−6036.

(20) Serier, H.; Gaudon, M.; Ménétrier, M. *Solid State Sci.* **2009**, *11*, 1192−1197.

(21) Kaul, A.; Gorbenko, O.; Botev, A.; Burova, L. *Superlattices Microstruct.* **2005**, *35*, 272−282.

(22) Zhang, X.; Pu, X.; Chen, Y.; Gu, X.; Xu, D.; Zhang, S. *Mater. Lett.* **2013**, *112*, 129−132.

(23) Iqbal, J.; Jan, T.; Ismail, M.; Ahmad, N.; Arif, A.; Khan, M.; Adil, M.; ul Haq, S.; Arshad, A. *Ceram. Int.* **2014**, *40*, 7487−7493.

(24) Fichtl, M. B.; Schumann, J.; Kasatkin, I.; Jacobsen, N.; Behrens, M.; Schlögl, R.; Muhler, M.; Hinrichsen, O. *Angew. Chem., Int. Ed.* **2014**, *53*, 7043−7047.

(25) Hegedüs, A. J.; Kiss, A. B. *Microchim. Acta* **1966**, *54*, 813−832.

(26) (a) Sloczynski, J.; Grabowski, R.; Kozlowska, A.; Olszewski, P. K.; Stoch, J. *Phys. Chem. Chem. Phys.* **2003**, *5*, 4631−4640. (b) Schumann, J.; Lunkenbein, T.; Tarasov, A.; Thomas, N.; Schlögl, R.; Behrens, M. *ChemCatChem* **2014**, *6*, 2889−2897.

(27) Kühl, S.; Tarasov, A.; Zander, S.; Kasatkin, I.; Behrens, M. *Chem. - Eur. J.* **2014**, *20*, 3782−3792.

(28) Ischenko, V.; Polarz, S.; Grote, D.; Stavarache, V.; Fink, K.; Driess, M. *Adv. Funct. Mater.* **2005**, *15*, 1945−1954.

(29) Djurisic, A. B.; Choy, W. C. H.; Roy, V. A. L.; Leung, Y. H.; Kwong, C. Y.; Cheah, K. W.; Rao, T. K. G.; Chan, W. K.; Lui, H. T.; Surya, C. *Adv. Funct. Mater.* **2004**, *14*, 856−864.

(30) Göpel, W. *J. Vac. Sci. Technol.* **1978**, *15*, 1298−1310.

(31) Vorobyeva, N.; Rumyantseva, M.; Vasiliev, R.; Kozlovskii, V.; Soshnikova, Y.; Filatova, D.; Baranchikov, A.; Ivanov, V.; Gaskov, A. *Russ. J. Inorg. Chem.* **2014**, *59*, 403−412.

(32) (a) Gabás, M.; Landa-Cánovas, A.; Luis Costa-Krämer, J.; Agulló-Rueda, F.; González-Elipe, A. R.; Díaz-Carrasco, P.; Hernández-Moro, J.; Lorite, I.; Herrero, P.; Castillero, P.; Barranco, A.; Ramón Ramos-Barrado, J. *J. Appl. Phys.* **2013**, *113*, 163709. (b) Gabás, M.; Torelli, P.; Barrett, N. T.; Sacchi, M.; Ramos Barrado, J. R. *APL Mater.* **2014**, *2*, 012112.

(33) Ginés, M. J. L.; Marchi, A. J.; Apesteguía, C. R. *Appl. Catal., A* **1997**, *154*, 155−171.

(34) Chinchen, G. C.; Spencer, M. S. *J. Catal.* **1988**, *112*, 325−327.

(35) Wang, G.-C.; Nakamura, J. *J. Phys. Chem. Lett.* **2010**, *1*, 3053−3057.

(36) Schumann, J.; Tarasov, A.; Schlögl, R.; Behrens, M. Unpublished results, 2015.

(37) Frost, J. C. *Nature* **1988**, *334*, 577−580.